About the vacuum UV photoabsorption spectrum of methyl fluoride (CH₃F): the fine structure and its vibrational analysis

R. Locht [a], B. Leyh [a,1], A. Hoxha [a], D. Dehareng [b], H.W. Jochims [c], H. Baumgärtel[c]

[a] *Département de Chimie Générale et de Chimie Physique, Institut de Chimie Bât. B6c, Université de Liège, Sart-Tilman par B-4000 Liège 1, Belgium*

[b] *Centre d'Ingéniérie des Protéines, Institut de Chimie, Bât. B6a, Université de Liège, Sart-Tilman par B-4000 Liège 1, Belgium*

[c] *Institut für Physikalische und Theoretische Chemie, Freie Universität Berlin, Takustraße 3, D-14195 Berlin, Germany*

Abstract

The vacuum UV photoabsorption spectrum of CH₃F has been recorded between 7 and 24 eV and has been analyzed in detail. Broad and structureless peaks are observed over the entire photon energy range. They are all assigned to transitions to Rydberg states, members of series converging successively to the $2e^{-1}$, $5a^{-1}$ and $1e^{-1}$ ionization limits. These features are underlying very long series of narrow and weak structures in the range of 10-13.2 eV. Through a continuum subtraction procedure, about 70 lines could clearly be identified. These have been assigned to long vibrational progressions belonging to Rydberg states corresponding to the $2e \rightarrow 3p$ and $2e \rightarrow 6s/5d$ configurations. These states are split by a Jahn-Teller distortion. Ab initio calculations lead to a Jahn-Teller stabilization energy of about 0.84 eV. The main features observed in the two bands are assigned to one single long vibrational progression of $hc\omega \sim 0.160$ eV (1 290 cm⁻¹) related to the C-F Jahn-Teller inactive stretching vibration. The remaining structure is assigned to the low excitation of the Jahn-Teller active vibrational modes, i.e. the bending modes v_5 and v_6 characterized by $hc\omega_5 \sim 0.120$ eV (970 cm⁻¹) and $hc\omega_6 \sim 0.082$ eV (660 cm⁻¹). Leaning on the present results and assignments previously reported photoelectron spectroscopic data on CH₃F⁺ [L. Karlsson, R. Jadrny, L. Mattsson, F.T. Chau, K. Siegbahn, Phys. Scripta 16 (1977) 225] have been reconsidered and reinterpreted.

1. INTRODUCTION

To get a deeper insight into the various aspects of the ionization and the monomolecular dissociation dynamics of molecular ions, we extensively investigate the photoabsorption spectrum, the He(I) and the threshold photoelectron (TPES) spectra, the constant ion state (CIS) spectra and the fragment ions translational energy release spectra in several types of molecules. Keeping this aim in mind, molecular systems e.g. ethylene and its various halogenated derivatives [1-5] and monohalogenated methanes [6] are being or have been investigated. Several of these studies [5, 7-9] showed the major importance of the localization and identification of neutral molecular states embedded in the ionization continua. In some cases, these states were shown to play a crucial role in the dissociation dynamics [6, 7, 10].

Though the halogen polysubstituted derivatives of methane have been thoroughly studied in the recent past by many groups [11-15][2] using most of the available spectroscopic techniques, the monosubstituted species received much less attention. Among the methyl monohalides, surprisingly the least investigated is the monofluorinated member CH₃F. Its photoabsorption spectrum has been reported a few times, as studied under different conditions.

---

[1] Chercheur Qualifié FNRS (Belgium).

[2] See also references therein.

First, Stokes and Duncan [16] photographed the photoabsorption spectrum of CH_3F in the vacuum UV region by using a He discharge source. The observed electronic transitions were classified in Rydberg series converging to the first two ionization limits, i.e. at 103 240 cm^{-1} (12.80 eV) and 123 200 cm^{-1} (15.27 eV). These authors observed a fine structure which they assigned to one vibrational progression. Edwards and Raymonda [17] examined the photoabsorption spectra of the fluoromethanes as excited by a Lyman line source. They only mentioned a vibrational structure without any further analysis. Sauvageau et al. [18] repeated this work using the Hopfield continuum and measured the molecular extinction coefficient ε_λ for the four fluoromethanes (CH_nF_{4-n} with n = 0-3). These authors also reported on the observation of a short vibrational progression, without further analysis. However, they mentioned a wave number of 400 cm^{-1} (0.050 eV) at about 10.6 eV and of 1000 cm^{-1} (0.124 eV) at about 11.2 eV. The publication of Wu et al. [19] is the only work, to our knowledge, extending the observation of the CH_3F photoabsorption to higher photon energies, i.e. above 11.8 eV (the LiF window limit), using synchrotron radiation. They measured the photoabsorption cross-section and analyzed the spectrum between 175 and 760 Å (16.3-70.8 eV).

Though usually less resolved in this energy range, the electron energy loss spectra are very useful for the study of molecular structure. The most recent work on CH_3F using this technique has been reported by Olney et al. [20]. They measured the photoabsorption oscillator strength between 7 and 250 eV. In a high resolution dipole (e,e) measurement in the range of 7.5-50 eV electron energy, they were able to resolve an extended fine structure but no further analysis was proposed.

We analyzed the photoabsorption spectrum of CH_3F in an earlier report [6] with the aim to search for the possible existence of superexcited states at 16.8 and 21.2 eV participating in the production of CH_3^+ fragment ions. No analysis of the low energy part of the spectrum was presented. The main goal of this paper is to report on a detailed reexamination of the photoabsorption spectrum recorded under improved conditions, as well as on an assignment of the extensive fine structure observed between 10 and 13 eV photon energy, based on new ab initio calculations.

2. EXPERIMENTAL

2.1. Experimental setup

The experimental setup used in this work will be described briefly. Synchrotron radiation available from the BESSY I facility (Berlin, Germany) is dispersed with a vacuum UV monochromator (beamline lm-NIM-2). This monochromator is a modified M-225 McPherson, with a focal length of 1.5 m (instead of 1 m in the commercial version). A laminar Zeiss grating is used for the efficient second spectral order reduction; it is gold coated with 1200 ℓ/mm. The width of the entrance and the exit slits of 100 µm provides a 0.1 nm wavelength resolution. The light passes through a 1 mm thick stainless steel microchannel plate to ensure a differential pressure of 1:1000 before entering a 30 cm long stainless steel absorption cell. The vapor pressure in this cell is measured by a Balzers capacitor manometer (1 mbar full range). The light is detected by a sodium salicylate sensitized photo-multiplier fixed at the end of the absorption cell opposite to the light entrance slit. Output pulses are recorded by a 100 MHz counter. The recording of an absorption spectrum requires one scan with gas in the absorption cell and one with an empty cell. The stability of the synchrotron radiation and of the pressure in the cell allowed us to ensure reliable absorption data. The spectra presented in the following sections are corrected for any pressure drift. The commercially available CH_3F, purchased from Matheson Company Inc., is used without further purification.

### 2.2. Data handling and error estimation

As will be noticed in the next section, most of the weak fine structures observed in these spectra is superimposed on fairly intense broad absorption peaks. A way to facilitate the detailed analysis of this structured part of the spectrum consists in a continuum subtraction. This procedure has already been successfully used earlier [21]. For this purpose, the experimental curve is severely smoothed to simulate the underlying continuum, which is subtracted from the original photoabsorption spectrum. The smoothing procedure consists in filtering the experimental curve by fast Fourier transform. The weak fine structure emerges as a series of sharp and strong peaks superimposed on a remaining very weak and slowly varying background. This procedure has been applied separately to the seven spectra recorded in this experiment under different pressure, resolution and recording conditions. Each structure mentioned in this work is present in all seven data sets. The energy position of the structures are averaged values over these seven independent measurements. The error, mentioned separately for

each level, is given by one standard deviation.

3. EXPERIMENTAL RESULTS

The photoabsorption curve of CH_3F has been measured over the photon energy range of 7-30 eV. Owing to its transmission curve, the cutoff limit of the grating used in this experiment lies at about 26 eV. Only the photon energy range of 7-24 eV will be discussed in this work. This photoabsorption spectrum is reproduced in Fig. 1 where the molar extinction coefficient ϵ_{hv} is given as a function of the photon energy (eV). A crude comparison with the data reported by Edwards and Raymonda [17] shows a fairly good agreement with the present measurement on ϵ_{hv}. These are somewhat underestimated with respect to the work of Sauvageau et al. [18]. In a more critical review, Olney et al. [20] made a quantitative comparison of photoabsorption cross-sections and oscillator strength over the 7-50 eV photon energy range. They showed that the values reported in the latter work [18] provide photoabsorption oscillator strength about 20%, too high at 14 eV as compared to the absolute values measured by high resolution dipole (e,e) measurements [20]. At 9.5 and 11.5 eV, this quantity lies between those deduced from the photoabsorption data [17,18].

Fig. 1. *Vacuum UV photoabsorption spectrum of CH_3F measured between 7.5 and 24.0 eV photon energy. The intensity is plotted in terms of molar extinction ε_{hv} in ℓ $(mol \; cm)^{-1}$.*
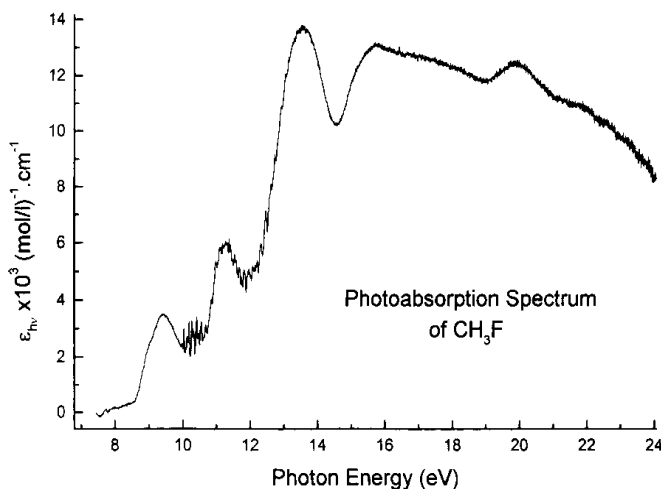
As clearly observed in Fig. 1, in the photon energy range of 9.5-14 eV, a weak but very well-defined fine structure is superimposed on intense broad peaks. On the other hand, at high energy (i.e. 15-24 eV), several weak and diffuse peaks are detected, superimposed on a strong continuum.

In order to analyze these features and to measure their energy level (wave numbers) as precisely as possible, we applied the procedure described in Section 2.2 to both energy ranges. The result is shown in Fig. 2(a) and (b), where the quantity Δ defined below is plotted as a function of the photon energy. This quantity Δ stands for the point-to-point difference between the original photoabsorption spectrum (PAS) and the strongly smoothed curve (SSPA) resulting from fast Fourier transform. Owing to the scattering of the signal in Fig. 2(b), a smoothed curve is drawn through the points.

The position in energy of the most salient features as defined by their maximum are listed in Table 1 together with the results of previous measurements.

The energy positions of the features observed in the first part of the fine structured photon energy range of 10.03-10.78 eV are listed in Table 5, together with previous measurements [16,23] mentioned here for comparison. Though being a photoelectron spectroscopic work, reference is made to the paper of Karlsson et al. [23] because these authors based their vibrational structure assignment in the first photoelectron band on the photoabsorption data of Stokes and Duncan [16]. The numbers listed in the last two columns of Table 5 will be discussed in the next section.

The remaining part of the fine structure observed in the photon energy range of 10.850-13.257 eV is gathered in Table 6. The first column contains few observations made in the first band of the He(I) photoelectron spectrum as reported by Karlsson et al. [23].

Fig. 2. *Fine structured part of the photoabsorption spectrum of CH_3F: (a) photon energy range of 9.7-14.0 eV and (b) photon energy range of 15.0-23.0 eV. See text for data handling procedure.*
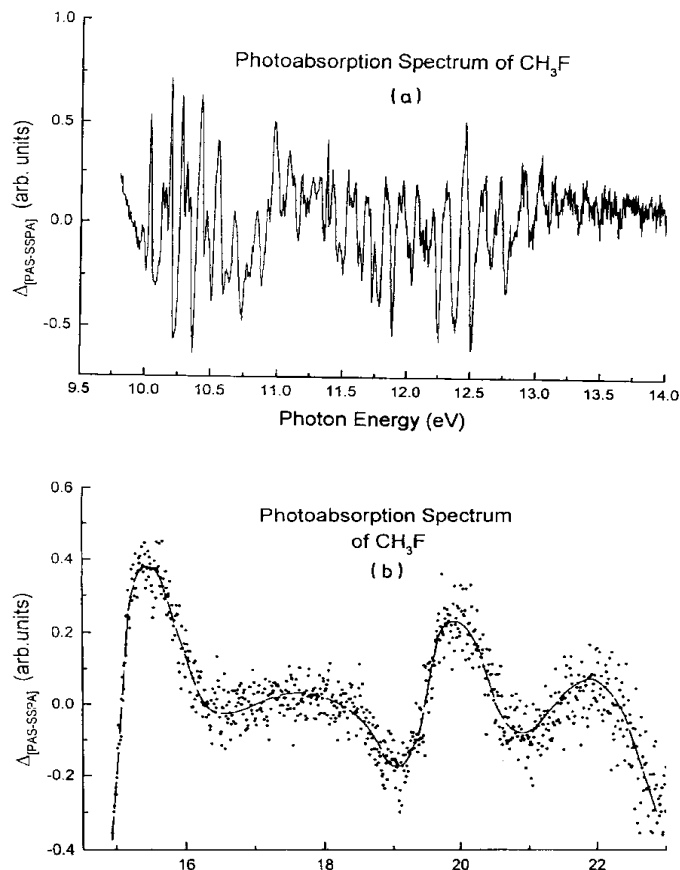
4. DISCUSSION

For the sake of clarity in the following discussion of the experimental results, the molecular orbital configuration of CH_3F in the C_{3v} group of symmetry has to be kept in mind i.e.

$$(1a_1)^2(2a_1)^2(3a_1)^2(4a_1)^2(1e)^4(5a_1)^2(2e)^4 : \widetilde{X}\,^1A_1$$

where the two first orbitals, i.e. $1a_1$ and $2a_1$ are the two inner-shell orbitals having essentially F(1s) and C(1s) character, respectively. The $3a_1$ and $4a_1$ orbitals correspond to the inner-valence orbitals, whereas the 1e, $5a_1$ and 2e orbitals correspond to the outer-valence orbitals. The He(I) [23] and He(II) [24] photoelectron spectra provide the vertical ionization energies at 13.04 eV corresponding to $(2e)^{-1}$, at 17.2 eV assigned to $(5a_1/1e)^{-1}$ and at 23.5 eV corresponding to $(4a_1)^{-1}$. These three energies are the possible convergence limits of the Rydberg series observed in the photoabsorption spectrum measured in the 7.0-24.0 eV photon energy range.

4.1. The main features

As shown in Fig. 1, the main features are broad bands for which only maxima can be determined. Their positions are listed in Table 1. Except for the data published by Wu et al. [19], who measured the photoabsorption of CH_3F above 16 eV only, all the measurements agree fairly well with each other. The electron

energy loss spectroscopic work of Harshbarger et al. [22] is consistent with the photoabsorption data.

The first peak observed at 9.37 eV, assigned to a 2e → 3s Rydberg transition with a term value of 3.64 eV and an effective quantum number $n^* = 1.925$, shows a shoulder on the low energy side at about 9.04 eV. Olney et al. [20] also reported on the existence of this feature in their high resolution dipole (e,e) measurement. By decomposition into Gaussian components, they determined two peaks with maxima at 8.94 and 9.40 eV successively. These authors assigned these features to the Jahn-Teller splitting of the electronic state resulting from the $2e^{-1}$ excitation on the basis of the corresponding splitting of 0.6 eV observed in the photoelectron spectrum [23].

Table 1- *Vertical excitation energies (EE_{vert}) (eV), vertical ionization energies (IE_{vert}) (eV) and assignments for the photoabsorption spectrum of monofluoromethane*

		EE_{vert}				IE_{vert}
Pabs[a] [16]	Pabs[a] [6]	(e,e)[b] [20]	EELS[c] [22]	This work	Assignment	[23,24]
-	-	[8.98]	-	9.04(s)	2e → 3s	
9.35	-	9.40	9.36	9.37		
-	-	10.0-10.8	-	10.0-10.8	2e → 3p	
10.58	-	-	10.42	10.04(m)		
-	-	11.0-11.9	-	10.8-11.8	2e → 3p	
11.37	11.20	-	11.21	11.27(m)	(continued)	
						13.04 $(2e)^{-1}$
-	-	-	-	11.8-13.2	2e → 6s/5d	
13.52	13.50	~13.4	13.41	13.57(m)	$5a_1$/1e → 3s and/or 3p	
-	15.25	~15	15.25	15.73	$5a_1$/1e → 4s/3d	
-	-	-				17.2 $(5a_1$/1e$)^{-1}$
			-	~17.9		
-	19.80	~19.5	19.78	19.9	$4a_1$ → 3s	
-	20.40	-	-	-		
-	22.30	-	-	22.0	$4a_1$ → 4s/3d	23.5 $(4a_1)^{-1}$
-	-	-	-	-		

[(s) and (m) refer to shoulders and maxima in the corresponding bands respectively.] [a]Pabs: photoabsorption spectroscopy. [b](e,e): dipole (e,e) electron spectroscopy. [c]EELS: electron energy loss spectroscopy.

The two first broad peaks at 9.37 and 11.27 eV, respectively, are separated by a progression for which the maximum is estimated to be at about 10.4 eV. On the basis of this energy and the convergence limit at 13.04 eV for the $2e^{-1}$ photoelectron band [23], an effective quantum number $n^* = 2.270$ is determined. This could indicate that one is dealing with a Rydberg state with a p-character. This energy region will be discussed in more detail in the next section.

The band at 11.27 eV is well defined but underlies a weak fine structure, which will be analyzed in the next section. The term value associated with this band is 1.77 eV and the effective quantum number is $n^* = 2.772$. Harshbarger et al. [22] and Olney et al. [20] assigned this band to a 2e → 4s/3d transition.

The strongest photoabsorption band of CH_3F has its maximum near 13.57 eV and spreads from 12.5 to 14 eV. As shown in Fig. 2(a), a fine structure extending to at least 13.2 eV is superimposed on this continuum. Separating the broad feature from the fine structure, the term value associated with the former is estimated at 3.63 eV and an effective quantum number $n^* = 1.936$ is obtained. This strongly suggests a ($5a_1$/1e) → 3s transition where the $5a_1$ and the 1e orbitals are nearly degenerate. On the basis of the peak width, Harshbarger et al. [22] suggested that within the energy range of 12.5-14 eV, ($5a_1$/1e) → 3s and ($5a_1$/ 1e) → 3p transitions should occur.

The energy range of the photoabsorption spectrum above 15 eV has been handled as described in Section 2.2. Despite the unfavourable signal-to-noise ratio resulting from this procedure, clearly four features can be observed: a peak at 15.7 eV, a very broad weak band at about 18 eV, which spreads over a photon energy range of about 3 eV, and finally peaks at 19.9 and at 22.0 eV.

The feature defined by its maximum at 15.7 eV spreads from about 15-17 eV and would have a term value of 1.47 eV with respect to the ionization limit at 17.2 eV. An effective quantum number $n^* = 3.04$ is

calculated. This probably indicates that this peak corresponds to a $(5a_1/1e) \rightarrow 4s/3d$ transition. This is in agreement with earlier reports [6, 20, 22]. This transition was also identified as being responsible for the dissociative autoionization producing thermal and nearly thermal CH_3^+ fragment ions when using the Ne(I) lines for ionization [6].

The very weak and broad structure following the peak at 15.7 eV overlaps the energy range of the $(5a_1/1e)^{-1}$ photoelectron band [24]. This feature is also observed in the photoabsorption spectrum reported by Wu et al. [19].

The two remaining structures observed at 19.92 and 22.01 eV are observed below the $(4a_1)^{-1}$ ionization limit. Their term values are 3.58 and 1.49 eV. The calculated effective quantum numbers are $n^* = 1.949$ and $n^* = 3.022$, which are indicative of $4a_1 \rightarrow 3s$ and $4a_1 \rightarrow 4s/3d$ transitions. These features were neither discussed nor assigned in previous papers [6, 19, 20, 22]. The latter Rydberg state overlaps the energy of the He(I) resonance line at 21.22 eV and its autoionization should be responsible for the production of the thermal and nearly thermal CH_3^+ fragment ions by dissociative autoionization induced by the He(I) resonance line [6].

4.2. The fine structure

4.2.1. Results of the ab initio calculations

In the most recent past, two quantum mechanical calculations were reported about CH_3F and CH_3F^+ [25,26]. Gauld and Radom [25] used high level ab initio calculations to describe CH_3X and CH_3X^+ (where X = F, Cl, OH, NH_2, SH and PH_2) and their isomeric species CH_2X^+H. They obtained their optimized geometries and thermochemical properties. Good agreement is found between theory and experiment for most of these species. Significant differences are mentioned for CH_3F^+ and its ylidionic isomer CH_2X^+H for which the authors suggest a revision of the experimental data.

Lugez et al. [26] investigated the infrared spectrum of the methyl halide cations trapped in a frozen neon matrix. The discussion is supported by ab initio calculations at MP2 as well as at QCISD levels. In agreement with Gauld and Radom [25], they also found a minimum for a CH_3F^+ cation distorted to the C_s symmetry and with a ground state of $^2A''$ electronic symmetry approaching the CH_2F^+H structure, where the C-F bond length is considerably shorter than in the neutral molecule. This is not surprising since the ground electronic state has a ^2E symmetry in the C_{3v} point group and will therefore be submitted to a Jahn-Teller distortion [27]. The main contribution of Lugez et al. [26] is the calculation of vibrational wave numbers in CH_3F^+ and the comparison of these values with their infrared data and with the values obtained for the cation by photoelectron spectroscopy [23]. In order to investigate in further detail, the Jahn-Teller interaction in CH_3F, it would be desirable to obtain informations on the $^2A'$ component for which no previous calculation is available.

Therefore, we performed ab initio calculations of CH_3F and CH_3F+ using the GAUSSIAN 94 program [28] at the MP2 and MP4 frozen core level [29,30][3] with 6-31G** basis sets [31,32]. The geometries are optimized for the C_{3v} and C_s symmetry groups. The results are shown in Table 2 for CH_3F ($\tilde{X}\,^1A_1$) and CH_3F^+ ($^2A''$ and $^2A'$) together with the results of previous calculations [25, 26].

An essential first result, which is consistent with previous ab initio calculations, is the severe shortening of the C-F bond length upon ionization in both the $^2A''$ and the $^2A'$ states. This fact will have important consequences on the vibrational analysis of the absorption spectrum. Furthermore, the Jahn-Teller distortion is found to act on both the bond length and the bond angles. This leads to the C_s symmetry, with two equivalent hydrogen nuclei called H2 (see figure in Table 2). As can be expected on the basis of the symmetry properties of the 2e orbital in the $^2A''$ state, the H2-C-H2 bond angle is reduced compared to the neutral molecule, whereas the reverse is true for in the $^2A'$ state. Important variations of the bond lengths are also observed (Tables 2 and 3). More particularly, the H2-C-F-H1 dihedral angle strongly deviates from 120 degree. Components of the energy gradient were calculated for both cationic states at the neutral ground state equilibrium geometry and these are listed in Table 3. The gradient preserves the C_s symmetry, imposing the symmetry of both the wave packet motion and the symmetry of the observed vibrational modes (a')· The vibrational wave numbers of the neutral molecule and of the $^2A''$ and $^2A'$ states of the cation have been calculated and weighted by the 0.937 empirical correction factor [33]. The results are displayed in Table 4 for CH_3F and CH_3F^+ ($^2A''$ and $^2A'$). The nuclear

---

[3] MP2/4 is the second/fourth order MØller-Plesset perturbation framework.

motions associated with the nine vibrational normal modes are described with reference to symmetry coordinates (ml to ml2) depicted in Fig. 3.

For the neutral CH_3F ($\tilde{X}\,^1A_1$) molecule, calculated and experimental wave numbers [34] agree satisfactorily. Despite a lowering in most cases with respect to the results of Lugez et al. [26], the wave numbers characterizing the $^2A''$ state of the ion are in fairly good agreement. The slight discrepancy could be ascribed to the difference of the calculation levels, i.e. MP2 in this work and QCISD in Ref. [26], and to the use of distinct basis sets.

Due to the threefold symmetry of the CH_3F system, three minima corresponding to the distorted $^2A''$ state exist and are generated by the cyclic permutation of the three hydrogen atoms. The $^2A'$ state has also been optimized (Table 2) and corresponds to the transition state linking two equivalent $^2A''$ minima. As expected, an intrinsic reaction path leads from such a transition state to either of the neighbor minima. To facilitate the understanding of the situation discussed here, Fig. 4 displays potential energy contour diagrams of the lower part of the Jahn-Teller split potential energy surface of the CH_3F^+ ($\tilde{X}\,^2E$) state. This diagram is derived from a perturbational treatment of the Jahn-Teller effect up to the second order [35]. The potential energy is given by the equation

$$V(q_x, q_y) = V(\Delta, \phi)$$
$$= E_0 - \lambda\Delta + [\mu - \tfrac{1}{2}v\sin(3\phi)]\Delta^2,$$

where q_x and q_y are degenerate symmetry coordinates which belong to the E irreducible representation of the C_{3v} point group. They correspond to the antisymmetrical bending motion. Δ and Φ are the polar coordinates corresponding to q_x and q_y. The numerical parameters λ, μ and v are chosen to reproduce the ab initio results for the energy of the minima ($^2A''$) and saddle points ($^2A'$) as well as the positions of the minima. The threefold symmetry is clearly observed. The energy stabilization brought about by the distortion, i.e. the energy difference between the C_{3v} apex and the minima is 0.84 eV at the MP4/6-31G** level. On the other hand, the saddle points are calculated to lie only 0.075 eV above the minima.

Table 2- *Optimized geometries of CH_3F ($\tilde{X}\,^1A_1$) in the C_{3v} symmetry group and CH_3F^+ ($^2A''$ and $^2A'$) in the C_s symmetry group calculated at different levels: distances in A and angles in degrees. Comparison is made with previous calculations at their highest levels [25, 26]*

Level	C-F	C-H1	C-H2	H1-C-F	H2-C-F	H2-C-F-H1
			CH_3F ($\tilde{X}\,^1A_1$) C_{3v}			
MP2/6-31G**	1.3893	1.0882	1.0882	109.26	109.26	120.0
MP4/6-31G**	1.3892	1.0892	1.0892	109.23	109.23	120.0
[25]	1.384	1.096	1.096	109.2	109.2	120.0
[26]	1.387	-	-	-	-	-
			$CH_3F^+(^2A'')$ C_s			
MP2/6-31G**	1.2943	1.0823	1.1574	116.82	109.60	138.92
MP4/6-31G**	1.2912	1.0831	1.1624	117.52	110.48	140.29
[25]	1.283	1.090	1.176	117.9	110.79	140.82
[26]	1.282	-	-	-	-	-
			$CH_3F+(^2A')$ C_s			
MP2/6-31G**	1.3177	1.2051	1.0960	101.70	112.62	105.72
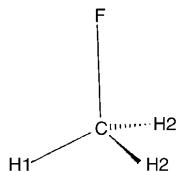
The wave numbers for the $^2A'$ state are about the same as those characterizing the $^2A''$ minimum but they involve different vibrational modes. This is due to the 120 degree rotation of the normal modes (Duschinski

effect) illustrated in Fig. 4. Obviously, an imaginary wave number (64li cm^{-1}) appears because one deals with a transition state. The corresponding mode has a m2 character (Fig. 3) and correlates therefore with the v_9 mode (a'' symmetry) of the ^{2}A'' minimum. The nuclear symmetry coordinate m2, which is a H-pivotal deformation motion (Fig. 3) is therefore the vibrational mode connecting with each other the different minima of the ground state potential energy surface. This means that among the possible Jahn-Teller active degenerate normal modes in the C$_{3v}$ point group, the deformation modes v_5 and/or v_6, which have components on m2 (Table 4), play an important role in the Jahn-Teller stabilization. The antisymmetric valence mode seems to play a minor role. This

Table 3 - *Gradient components ∂E/∂X, in Hartree/Bohr or Hartree/degree, for the ^{2}A'' and ^{2}A' states of CH$_3$F$^+$, respectively, calculated at the equilibrium geometry of the ground state CH$_3$F ($\tilde{X}$ ^{1}A$_1$)*

State	X					
	C-F	C-Hl	C-H2	Hl-C-F	H2-C-F	H2-C-F-H1
^{2}A''	-0.0349	-0.0025	+0.0197	-0.0172	-0.0233	+0.0301
^{2}A'	-0.0349	+0.0280	+0.0045	-0.0262	-0.0187	-0.0301

Table 4 - *Vibrational normal modes and their corresponding wave numbers (cm^{-1}) resulting from ab initio calculations at the MP2(FC)/6-31G** level, for CH$_3$F ($\tilde{X}$ ^{1}A$_1$) and CH$_3$F$^+$ (^{2}A'' and ^{2}A'), respectively in the C$_{3v}$ and C$_s$ symmetry group^a*

Designation	Wave number (this work)	Mode Description (see Fig. 3)	Ref. [34]
	CH$_3$F ($\tilde{X}$ ^{1}A$_1$) (C$_{3v}$)		
	a$_1$ Symmetry		
v_1	2936	m8	2964
v_2	1456	m3	1475
v_3	1042	m12	1048
	e Symmetry		
v_4	3033	m12	2982
v_5	1465	m2 + m6	1471
v_6	1150	m2 + m1	1195
	CH$_3$F$^+$(^{2}A'')(C$_S$)		Ref. [26]
	a' Symmetry		
v_1	3116	m9	3228
v_2	2479	m10	2589
v_3	1422	m4 + m5	1478
v_4	1283	m12	1321 v
v_5	1032	m1	1082
v_6	667	m6	808
	a'' Symmetry		
v_7	2217	m11	2190
v_8	1002	m2	1043
v_9	747	m2	1024
	CH$_3$F$^+$(^{2}A')(C$_S$)-TS		
	a' Symmetry		
v'_1	2896	m8	-
v'_2	2423	m9(+m6)	-
v'_3	1405	m3	-
v'_4	1323	m7	-
v'_5	1141	m12 + m5	-
v'_6	733	m4 + m5	-
	a'' Symmetry		
v'_7	2961	m11	-
v'_8	1151	antisymm m1	-
v'_9	i641	m2	-

^{a}The ^{2}A' component corresponds in fact to a transition state (TS). All wave numbers are corrected by the coefficient proposed by Scott and Radom [33].

is confirmed by the absence of this mode in the vibrational progressions which will be discussed in Section 4.2.2.On the basis of the geometrical differences between the cationic and the neutral states, the following vibrational motions should be excited upon ionization to the $^2A''$ state. According to Tables 2, 3 and Fig. 3, these would be: ml2 (C-F stretch), ml0 (C-H antisymmetric stretch), ml (CH$_3$-rock-ing), m4, m5 (H1/H2-C-F bend), m6 (H2-C-H2 bend) and m7 (H1-C-H2 pinch). Consequently, the following frequencies are expected to show up: v_4, v_2, v_5, v_3 and v_6. The observation of the gradient components confirms this analysis. It has to be noticed that the assignment of small frequencies has to be done cautiously because these are the least accurate.

Fig. 3. *Schematic representation and description of nuclear symmetry coordinates mi of CH$_3$X$^+$ in the C$_s$ symmetry group.*
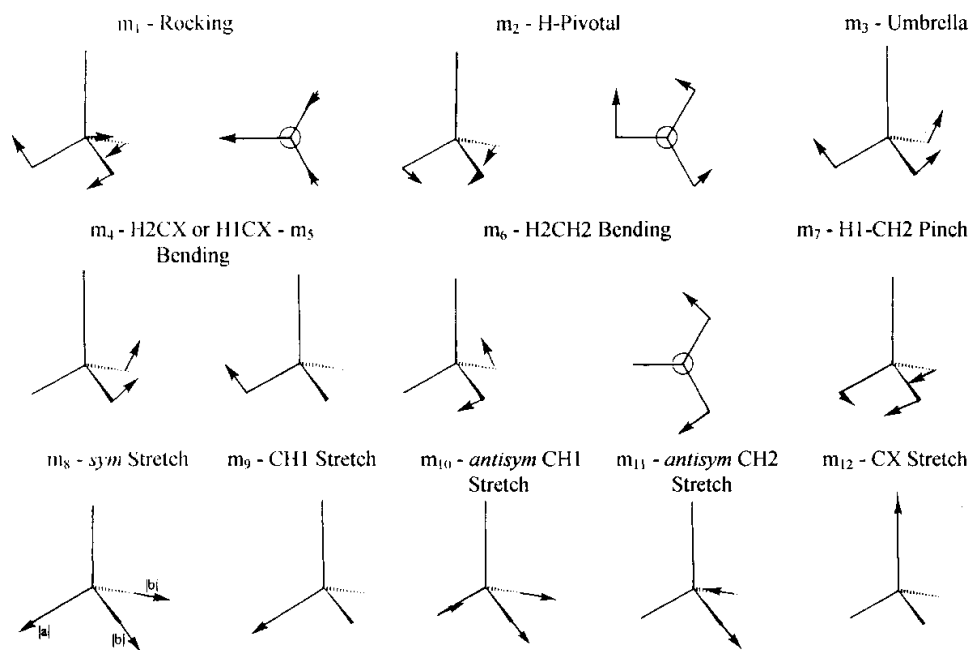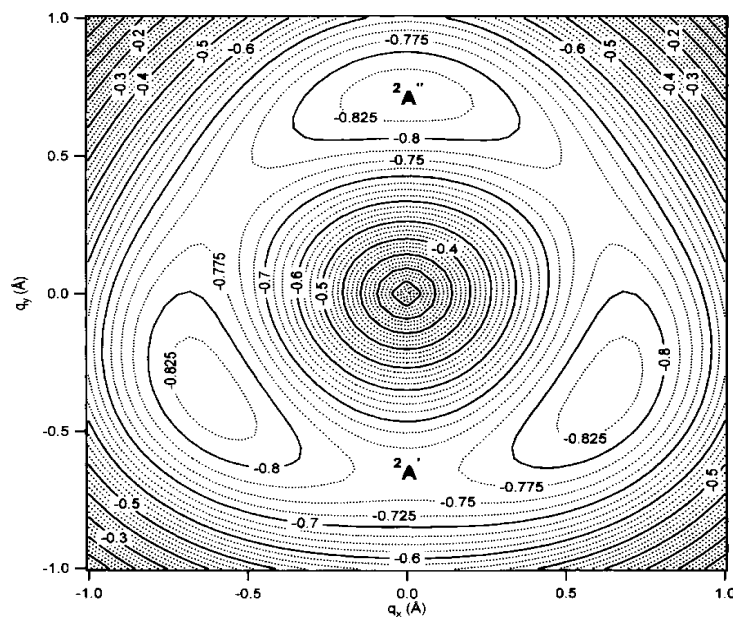

Fig. 4. *Contour lines of the low energy part of the Jahn-Teller distorted potential energy surface of the CH$_3$F+ X^{2}E state. The energies (eV) are given with respect to the apex (undistorted position). This diagram corresponds to a second-order perturbation treatment of the Jahn-Teller effect [35] (see text).*

4.2.2. The experimental data

The attention will be focussed here on the long series of weak structures observed between 10.0 and 13.2 eV photon energy as shown in Figs. 1 and 2(a). Only the first 15 peaks have been reported, analyzed and assigned in the literature [16] as shown in the first column of Table 5. Photoelectron spectroscopic data and assignments from Karlsson et al. [23] have been added as being useful for the interpretation. The results of this work are listed in the third and fourth columns in wave number (cm^{-1}) and energy (eV), respectively.

To avoid any confusion, it should be mentioned that the assignments made in Table 5 and in this discussion are based on the vibrational mode descriptions corresponding to the results of the ab initio calculations as presented in Section 4.2.1. The assignments presented in Ref. [23] result from the description of the vibrational modes in CH_3F^+ in terms of those of CH_3F in the C_{3v} group of symmetry.

Table 5- *Vibrational fine structure and energy levels observed in the 10.035-10.783 eV photon energy range*

Ref. [16][a]	Ref. [23][a,b,c]	This work			
		cm$^{-1(e)}$	eV[d]	n^{*e}	Assign.
80995	80940[b]	80940	10.035(4)	2.344	0-0
-	81633	81714	10.131(6)	2.357	v_6
81972	819	899	10.154(5)	2.357	v_5
82260	82254	82206	10.192(6)	2.331	$1v_4$
-	561	-	-	-	-
941	883	859	10.273(5)	2.332	$v_4 + v_6$
83 221	83 101	83 198	10.315(7)	2.339	$v_4 + v_5$
474	545	408	10.341(7)	2.329	$2v_4$
-	827	-	-	-	-
84187	84125	84077	10.424(5)	2.331	$2v_4 + v_6$
438	359	432	10.468(5)	2.337	$2v_4 + v_5$
669	746	577	10.486(4)	2.324	$3v_4$
85179	85013	85142	10.556(7)	2.341	$3v_4 + v_6$
338	367	650	10.619(2)	2.342	$4v_4$
783	-	-	-	-	-
86276	86166	86174	10.684(8)	2.334	$4v_4 + v_6$
919	561	-	-	-	-
87 438	87 263	973	10.783(8)	2.316	$4v_4 + 2v_6$

Comparison with previous measurements by photoabsorption [16] and photoelectron spectroscopy [23]. The value of the effective quantum number n* and the proposed assignments are inserted.
[a] In cm^{-1} units.
[b] Obtained by adding the vibrational spacings reported by [23] to 80 940 cm^{-1}.
[c] Recommended energy (eV) to wave number conversion factor: 1 eV = 8065.48 cm^{-1} [36].
[d] Numbers in brackets = one standard deviation (for explanation see text).
[e] Using the recommended value for the Rydberg constant, R = 13.6058 eV [36].

The comparison of the energy levels of the structures shows some significant discrepancy. The results of Stokes and Duncan [16] are reported as being affected by an error of about ± 10 cm^{-1}, when sharp bands are concerned. The maximum error allowed in the photoelectron spectroscopic work [23] is about 6 meV or 48 cm^{-1}. The standard deviation affecting each peak position in the present work is listed in Table 5 and ranges between 2 and 8 meV or 16-64 cm^{-1}. Despite these observations, very scarce are the overlapping measurements. The origin of this discrepancy is not easy to identify. A systematic error, e.g. monochromator calibration, seems to be very unlikely. Nevertheless, the corresponding features in each experiment can be identified unambiguously.

The series of narrow peaks starting at 10.035 eV has to be assigned as pertaining to vibrational progressions of one isolated Rydberg state. Indeed, taking the energy levels of the absorption spectrum and using the ionization energies reported by Karlsson et al. [23] as their respective convergence limit, an average term value of 2.500 ± 0.015 eV and an effective quantum number n^* = 2.333 ± 0.030 have been obtained by averaging over the 14 values.

The fine structure can be assigned on the basis of three vibrational normal modes of a' symmetry (C_s point group) in the 2e → 3p Rydberg state converging to the $^2A''$ ionic state, i.e. v_4(a') (C-F stretch), v_5(a') (CH$_3$ rock) and v_6(a') (H-C-H bend) using the notations resulting from the ab initio calculations (Section 4.2.1) and the conventional classification [34]. The two latter modes correlate to the v_5 and v_6 degenerate modes in the C_{3v}

group (Table 4) and are therefore Jahn-Teller active. On the other hand, the v_4 mode correlated to the v_3 mode in the C_{3v} point group does not lead to a symmetry lowering. Stokes and Duncan [16] designated the present $v_4(a')$ and $v_5(a')$ modes by the $v_2(a_1)$ and $v_3(a_1)$ modes. These authors did not observe the wave number corresponding to the actual $v_6(a')$ normal mode characterized by $hv_6 = 0.086 \pm 0.010$ eV ($\omega_6 = 690 \pm 80$ cm^{-1}). This vibrational energy has been observed in the photoelectron spectrum [23]. The absence of this vibration changes the assignment considerably [16]. The fact that v_2, corresponding to an antisymmetric C-H stretch, is not observed confirms the minor role played by this vibration in the Jahn-Teller stabilization, as already inferred from the ab initio results.

Up to 10.341 eV, the wave numbers obtained from the present photoabsorption spectrum are in full agreement with the photoelectron data of Karlsson et al. [23] but the assignment is completely different. Associated with the v_3, v_6 and v_5 vibrational progressions in the C_{3v} point group, in the present work, we suggest the following assignment $hc\omega_6 = 0.086 \pm 0.010$ eV ($\omega_6 = 690 \pm 80$ cm^{-1}), $hc\omega_5 = 0.121 \pm 0.009$ eV ($\omega_5 = 976 \pm 72$ cm^{-1}) and $hc\omega_4 = 0.157 \pm 0.010$ eV ($\omega_4 = 1266 \pm 80$ cm^{-1}). These values have to be compared with those reported by Karlsson et al. [23] of 0.086, 0.109 and 0.163 eV. In their photoabsorption spectrum, Stokes and Duncan [16] determined 975 cm^{-1} (0.121 eV) and 1278 cm^{-1} (0.158 eV). As mentioned earlier, the value of 0.086 eV is missing in this latter work. Karlsson et al. [23] based their assignment on a comparison between the wave numbers of the neutral and the ionized methyl fluoride. This ignores the strong modifications brought about in the vibrational force field by the ionization process, and in this case, by the Jahn-Teller effect. As an example, these authors [23] assigned the 86 meV transition energy to the C-F stretch. Such a decrease of the C-F wave number in the ion compared to the neutral cannot be maintained because the ab initio calculations unambiguously show that the involved 2e orbital has a CF antibonding character. The removal of an electron from this orbital leads therefore to an important C-F bond length shortening of 0.1 A and to an increase of the C-F stretching wave number whose calculated value of 0.159 eV (1283 cm^{-1}) is very close to the experimental value. Such a very good agreement between theory and experiment is also found for the two other intervals detected in the spectra, i.e. $hc\omega_6 = 0.083$ eV (667 cm^{-1}) and $hc\omega_5 = 0.128$ eV (1032 cm^{-1}).

However, two transitions which are observed in the ion [23] are detected neither in the present study, nor in Stokes and Duncan's work [16]. Moreover, two transitions detected by Stokes and Duncan [16] and/or by Karlsson et al. [23] are not observed in our spectrum. They would involve combinations $v_6 + v_5$, $v_6 + v_5 + v_4$. The combination reported at 86 561 cm^{-1} for $v_3 + 4v_5$ [23] has been allocated preferentially to the structure at 10.684 eV (Table 5), i.e. $v_6 + 4v_4$. An argument favoring this assignment is the value of the effective quantum number of $n^* = 2.334$, calculated as based on this assumption, which is very close to the average value of $n^* = 2.333 \pm 0.030$.

Fig. 5. *Birge-Sponer plot corresponding to the v_4 vibrational mode in the 10.03-10.78 eV photon energy range.*
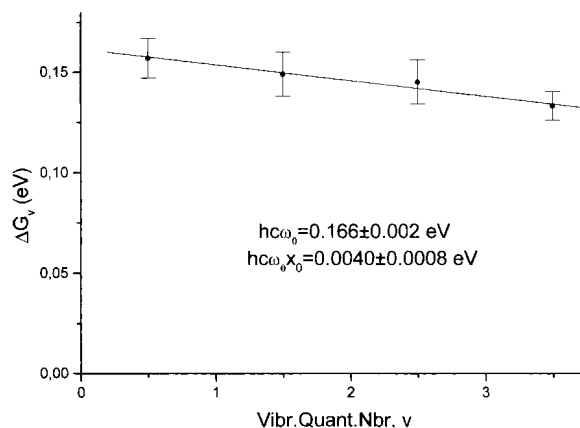
Furthermore, the fairly good precision on the present measurements clearly showed an anhar-monicity on the v_4 mode, observed up to $v = 4$. Karlsson et al. [23] already mentioned that the photoelectron band structure includes a small an-harmonicity. The Birge-Sponer plot related to this vibrational progression is shown in Fig. 5. A linear regression fitted the data with a correlation coefficient of 0.989, including the errors on ΔG_V. From the zero extrapolation and slope, the molecular constants $(hc\omega_0)_4 = 0.166 \pm 0.002$ eV $[(\omega_0)_4 = 1339 \pm 16$ cm$^{-1}]$ and $(hc\omega_0x_0)_4 = 0.0040 \pm 0.0008$ eV $[(\omega_0x_0)_4 = 32 \pm 6$ cm$^{-1}]$ have been derived.

After a drop of the relative intensities (Fig. 2(a)), the structures observed above 10.850 eV have increasing intensities reaching a maximum at about 11.007 eV and then slowly decrease for photon energies increasing to 12.0 eV. The density of structures in this energy range is much higher than that at lower energies.

As mentioned in the fourth column of Table 6, the effective quantum number which could be allocated to the structures observed in the present photoabsorption spectrum remains quite constant and close to the earlier obtained average of $n^* = 2.333 \pm 0.030$. This result could be obtained by relating the present spectrum with the remaining structures observed in the $\tilde{X}\ ^2E$ band of the photoelectron spectrum of CH_3F [23] and listed in the first column of Table 6. It is noteworthy to mention that in this energy range, the uncertainty on the energy levels as mentioned by the authors [23] is 10 meV (80 cm^{-1}) instead of 6 meV at most on the low energy side of the same band.

It is therefore suggested that this series of peaks belongs to the same $2e \rightarrow 3p$ Rydberg transition. Karlsson et al. [23] assigned the high energy part of the $\tilde{X}\ ^2E$ band of the photoelectron spectrum to the upper part of the Jahn-Teller split potential energy surface. However, a clear-cut transition between the two regimes is observed neither in our absorption spectrum nor in the photoelectron spectrum [23]. Therefore, we prefer to suggest an alternative detailed interpretation of the observed vibrational pattern based on the fact that most of the peaks measured up to 11.9 eV can be assigned as members of the nv_4 progression with the wave number and anharmonicity constant derived from the Birge-Sponer plot of Fig. 5. Fig. 6 displays the new Birge-Sponer plot obtained by considering nv_4 vibrational levels up to $n = 18$. The constants derived from the least squares fit, i.e. $(hc\omega_0)_4 = 0.157 \pm 0.003$ and $(hc\omega_0 x_0)_4 = 0.0035 \pm 0.0004$ eV, are very close to those derived from the first four levels. The correlation coefficient is 0.977. In addition, as this wave number refers to the C-F stretch, the dissociation energy deduced from the wave number and anharmonicity should not be very different from or converge to the $CH_3F^+ \rightarrow CH_3^+ + F$ dissociation energy. Even though such an extrapolation based on only one anharmonicity term is not expected to be very accurate, a value of 1.694 eV is obtained, and is consistent with the dissociation energy of 2.0 eV derived from photoionization mass spectrometric measurements [6]. A long progression associated with the C-F vibration is perfectly consistent with the important change in the C-F bond length, which is the largest change brought about upon ionization (Tables 2 and 3).

Besides this main vibrational progression, two other spacings have been identified above 10.85 eV, i.e. $\Delta G_V = 80 \pm 8$ meV (645 $\pm$ 60 cm^{-1}) and $\Delta G_V = 119 \pm 6$ meV (960 $\pm$ 50 cm^{-1}) as averaged over 14 and 10 values, respectively. These spacings can be assigned to the already mentioned Jahn-Teller active v_6 and v_5 modes. The fact that only low excitations of the Jahn-Teller active modes are observed implies that the wave packet only explores the lowest part of the Jahn-Teller split potential energy surface. As the potential well is relatively deep (0.84 eV), the wave packet does not come too close to the region where the Born-Oppenheimer approximation breaks down, i.e. where vibronic couplings are strong. This gives rise to the observed regular vibrational pattern.

The overall intensity in this band seems to decrease when the photon energy reaches about 12.0 eV. At this energy, lines are still observed at 11.913 and 11.939 eV (Table 6). Considering that these structures still correspond to vibronic transitions to the same $2e \rightarrow 3p$ Rydberg state characterized by the same effective quantum number $n^* = 2.333$, an ionization energy of 14.44 eV is calculated for the convergence limit of the 11.939 eV level. This energy is close to the Franck-Condon limit estimated for the $\tilde{X}\ ^2E$ photoelectron band of CH_3F [23] and is indicated in brackets in Table 6. Perhaps the very weak line at 12.025 eV still belongs to this progression and could fit a $nv_4 + v_5$ or $v_6 (n \geq 18)$, as indicated in Table 6.

The fine structure displayed upon the photo-absorption band at 11.27 eV is observed well beyond the Franck-Condon limit estimated at about 12 eV as shown in Fig. 2(a) and Table 6. This structure has likely to be assigned to a $2e \rightarrow ns/ (n-1)d$ or np transition and is superimposed on the $5a_1/1e \rightarrow 3s$ and/or $3p$ Rydberg transitions mentioned earlier. Considering our observations at lower energies, we expected to find about the same progressions.

As shown in Table 6, for all the remaining structures, which could be correlated with the vibrational progression of the photoelectron spectrum of CH_3F [23], about the same effective quantum number is obtained. Using 20 values, an average value of $n^* = 5.010 \pm 0.074$ is determined. In this photon energy region, a larger scattering of the energy level measurements has to be noticed and is marked by a larger standard deviation. This is essentially ascribed to a larger crowding of the structure. Nevertheless, this value of n^* is typical for a 6s/5d transition. However, an uncertainty remains concerning the lowest excitation energy to this Rydberg state. Using the 11.976 eV line and 12.533 eV for the adiabatic ionization energy, an $n^* = 4.942$ is calculated. It cannot be excluded that the actual lowest excitation energy should be at 11.991 eV using $n^* = 5.010$ and which should be buried in the 11.976 and 12.025 eV peaks. Some recordings showed a shoulder at this energy.

Table 6 - *Vibrational structure and energy levels observed in the 10.850-13.257 eV photon energy range*

Ref. [23][a]	This work			
	cm^{-1b}	eV^{b,c}	n^{*d}	Assignment
13.360	87 513	10.850(8)	2.328	$6v_4$
13.450	88 158	10.930(6)	2.323	$6v_4 + v_6$
13.487	533	10.979(8)	2.329	$7v_4$
-	779	11.007(2)	-	$6v_4 + 2v_6$
13.560	89 046	11.040(4)	2.323	$6v_4 + v_5 + v_6$
-	465	11.095(7)	-	$8v_4$
13.630	699	11.121(8)	2.329	$7v_4 + 2v_6$
-	90 175	11.180(2)	-	$9v_4$
-	392	11.207(8)	-	$8v_4 + v_5$
-	578	11.230(5)	-	$7v_4 + 3v_6$ or $7v_4 + 2v_5$
13.760	901	11.270(4)	2.337	$10v_4$
	91 199	11.307(13)		$9v_4 + v_5$
	554	11.351(9)		$11v_4$
	804	11.382(6)		$10v_4 + v_5$
	92 151	11.425(7)		$12v_4$
	594	11.480(8)		$13v_4$
	93 159	11.550(2)		$14v_4$
	619	11.607(14)		$15v_4$
	858	11.637(8)		$16v_4$
	94 143	11.672(16)		$17v_4$
	288	11.690(6)		$15v_4 + v_6$
	466	11.712(7)		$18v_4$
	853	11.760(3)		$16v_4 + v_5$
	95 530	11.844(7)		$17v_4 + 2v_6$
	96 087	11.913(5)		$18v_4 + v_5 + v_6$
[14.439]^e	294	11.939(9)	[2.33]^e	$18v_4 + 2v_5$
	595	11.976(7)		$18v_4 + 3v_6$
12.533			4.942	0-0 2e $\rightarrow$ 6s/5d
12.533		[11.991]^e	[5.01]^e	[0-0 2e $\rightarrow$ 6s/5d]^e
	96 990	12.025(4)		[$nv_4 + v_5(v_6)$ with $n > 18$]^e
12.619	97 482	12.086(4)	5.052	v_6
12.642	821	12.128(6)	5.145	v_5
12.696	98 031	12.154(6)	5.010	$1v_4$
12.734	466	12.208(9)	5.086/	$v_5 + v_6$
12.774			4.903	
12.801	99 095	12.286(6)	5.140	$v_4 + v_5$
12.850	305	12.312(9)	5.029	$2v_4$
12.891	418	12.326(3)	4.907	$v_4 + 2v_6$
12.928	-	[12.398]		$(2v_4 + v_6)$
12.960	-	[12.433]		$(2v_4 + v_5)$
13.005	100 507	12.461(8)	5.001	$3v_4$
13.038	725	12.488(5)	4.974	$2v_4 + 2v_6$
13.080	101 281	12.557(12)	5.100	$3v_4 + v_6$
13.181	555	12.591(7)	4.942	$4v_4$
-	102 096	12.658(2)		$3v_4 + v_5 + v_6$
13.230	338	12.688(8)	5.010	$4v_4 + v_6$
	612	12.722(4)		$5v_4$
13.320	806	12.746(7)	[4.869]	$4v_4 + 2v_6$
	103 169	12.791(7)	[5.071]	$4v_4 + v_5 + v_6$
13.360	507	12.833(13)	5.081	$6v_4$
	830	12.873(8)		$4v_4 + v_5 + 2v_6$

(continued on next page)

Table 6 *(continued)*

Réf. [23][a]	This work			
	cm$^{-1\ b}$	eV^{b,c}	n^{*d}	Assignment
13.450	104 056	12.901(5)	4.978	$5v_4 + 2v_6$
13.487	249	12.925(5)	4.920	$7v_4$
	645	12.974(4)		$5v_4 + 2v_5$
13.560	983	13.016(7)	5.001	$7v_4 + v_6$
	105 137	13.035(2)		$8v_4$
13.630	435	13.072(2)	[4.937]	$6v_4 + 3v_6$
	588	13.091(2)	[5.024]	$7v_4 + 2v_6$
	106 105	13.155(10)		$8v_4 + v_5$
13.760	468	13.200(10)	4.929	$10v_4$
	927	13.257(10)		$8v_4 + 2v_5$

Effective quantum numbers and assignments proposed in this work are also inserted.
[a] Ionization energies (eV) as reported in Ref. [23].
[b] Recommended energy (eV) to wave number conversion factor 1 eV = 8065.48 cm^{-1} [36].
[c] Number in brackets = one standard deviation (see text for explanation).
[d] Using the recommended value of the Rydberg constant R = 13.6058 eV [36].
[e] Data in square brackets, see text.

Fig. 6. *Birge-Sponer plot corresponding to the v_4 vibrational mode in the 10.03-11.91 eV photon energy range.*
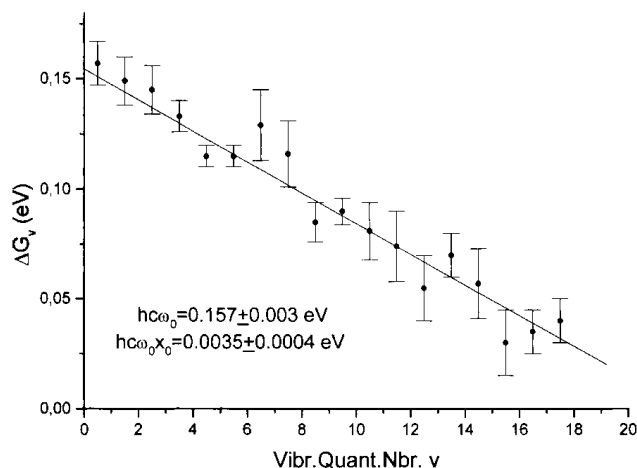
On the basis of a nearly equal effective quantum number, the features starting at 12.086 up to 13.257 eV are therefore assigned to one and the same progression of the 2e → 6s/5d Rydberg state. A possible assignment of the lines observed be tween 12.025 and 12.746 eV is reported in Table 6. An argument favoring this assignment, as well as the choice of the lowest excitation energy at 11.991 eV, is the possibility to determine a progression of the v_4 normal mode. Combinations with v_6 and v_5 vibrations are also observed. Furthermore, an anharmonicity is again observed in this band. A Birge-Sponer plot for 10 vibrational quanta is shown in Fig. 7. A linear regression could be fit to these data with a correlation coefficient of 0.987. This provides the molecular constants $(hc\omega_0)_4 = 0.167 \pm 0.004$ eV [$(\omega_0)_4 = 1348 \pm 30$ cm^{-1}] and $(hcx_0\omega_0)_4 = 0.0043 \pm 0.0007$ eV [$(\omega_0x_0)_4 = 35 \pm 6$ cm^{-1}]. These values are both in good agreement with the values determined earlier for the 2e → 3p transition, i.e. 0.157 ± 0.003 and 0.0035 ± 0.0004 eV.

Fairly good correlation is observed between the remaining high energy structures from 12.791-13.257 eV and the photoelectron spectrum. A few additional lines are observed in the photoabsorption spectrum. A complete assignment has been attempted (Table 6).

Fig. 7. *Birge-Sponer plot corresponding to the v_4 vibrational mode in the 11.99-13.25 eV photon energy range.*
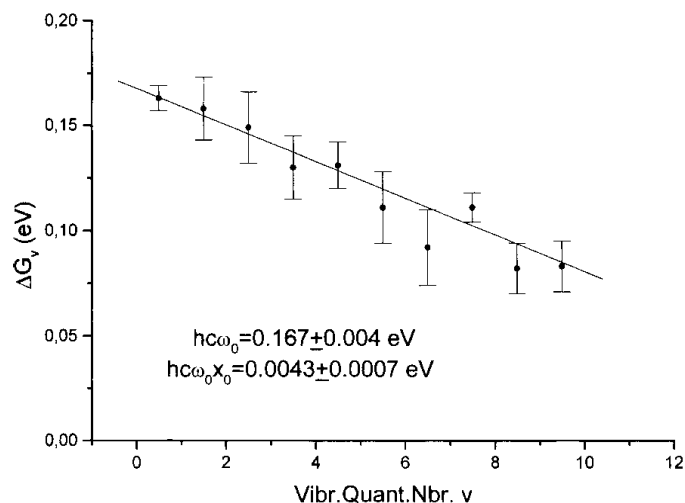
5. CONCLUSIONS

The vacuum UV photoabsorption spectrum of CH_3F has been examined in detail. It consists of broad peaks underlying many line shaped structures. The attention has particularly been focused on the fine structure observed between 10.03 and 13.25 eV. It has been assigned to two extended vibrational progressions associated with two Rydberg transitions, i.e. $2e \rightarrow 3p$ and $2e \rightarrow 6s/5d$. Ab initio calculations have been performed and the Jahn-Teller distortion accompanying the 2e Rydberg excitation in both bands is carefully considered. The main feature is assigned to one extended vibrational progression involving the Jahn-Teller inactive v_4 mode for which $hc\omega_0 \simeq 160$ meV (1290 cm^{-1}) and $hc\omega_0x_0 \simeq 4$ meV (32 cm^{-1}). Besides this motion, two Jahn-Teller active vibrational motions are slightly excited, i.e. v_5 and v_6 for which $hc\omega_5 \simeq 120$ meV (970 cm^{-1}) and $hc\omega_6 \simeq 82$ meV (660 cm^{-1}). Furthermore, a Jahn-Teller stabilization energy of 0.84 eV is theoretically predicted.

Fig. 8. *Birge-Sponer plot built on the data related to the first photoelectronic band of the CH_3F^+ ($\tilde{X}^2E$) cation as reported by Karlsson et al. [23] (for explantion, see text).*
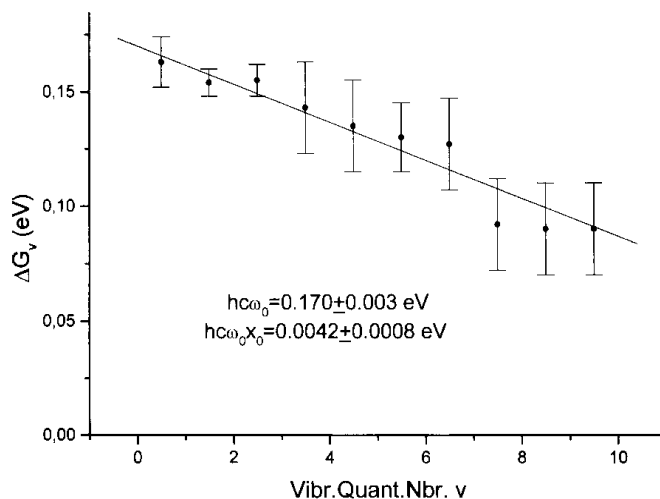
In the light of the present analysis, we are able to reconsider the interpretation of the photoelectron spectroscopic data published by Karlsson et al. [23]. Using their own data (see Table 2 in Ref. [23]) and by calculating the missing data by the Rydberg formula, a Birge-Sponer diagram has been plotted for the CH_3F^+ ($\tilde{X}^2A''$) state. Vibrational quanta up to $n = 10$ of the v_4 motion are found to be excited. The result is shown in

Fig. 8 and the molecular constants derived from this least squares fit are $(hc\omega_0)_4$ = 0.170 ±0.003 eV (1371 ± 24 cm^{-1}) and $(hc\omega_0 x_0)_4$ = 0.0042 ± 0.0008 eV (34 ± 6 cm^{-1}). This wave number has obviously to be assigned to the C-F stretching motion in agreement with ab initio calculations predicting an important C-F bond shortening. This description differs from the analysis of Karlsson et al. [23], who related this motion to the 0.086 eV quantum. In the present work, this latter energy is assigned to the antisymmetric bending motion v_6. These results are summarized in Table 7.

In the fourth column, the assignment proposed by Karlsson et al. [23] is reproduced, although we suggest a different interpretation, which is presented in the last three columns.

Table 7 - *Vibrational energies (meV) and assignments for CH$_3$F ($\tilde{X}$ $^1A_1$) and CH$_3$F$^+$ ($\tilde{X}$ $^2A''$) as determined by ab initio calculations, infrared spectroscopy [34], photoelectron spectroscopy [23] (for explanation, see text) and photoabsorption spectroscopy in this work*

Motion	Symmetry Group C$_{3v}$			Symmetry Group Cs		
	Mode	Th./exp. [34] CH$_3$F	CH$_3$F$^+$ [23]	Mode	Abs. Sp. This Work Rydberg	Theor. This Work CH$_3$F$^+$
C-F stretch	v_3	129/130	86	v_4	160	159
CH$_3$ rock	v_6	143/149	109	v_5	120	128
CH$_2$ bending	v_5	182/182	163	v_6	82	83

References

[1] G.Tornow, R.Locht, R.Kaufel, H.Baumgärtel, H.W. Jochims, Chem. Phys. 146 (1990) 305.

[2] R. Locht, B. Leyh, K. Hottmann, H. Baumgärtel, Chem. Phys. 220 (1997) 207.

[3] R. Locht, B. Leyh, K. Hottmann, H. Baumgärtel, Chem. Phys. 220 (1997) 217.

[4] A. Hoxha, R. Locht, B. Leyh, D. Dehareng, K. Hottmann, H. Baumgärtel, Chem. Phys. 256 (2000) 239.

[5] J. Momigny, R. Locht, Chem. Phys. Lett. 211 (1993) 161.

[6] R. Locht, J. Momigny, E. Rühl, H. Baumgärtel, Chem. Phys. 117 (1987) 305.

[7] A. Hoxha, R. Locht, A.J. Lorquet, J.C. Lorquet, B. Leyh, J. Chem. Phys. 111 (1999) 9259.

[8] K.M. Weitzel, F. Güthe, J. Mähnert, R. Locht, H. Baumgärtel, Chem. Phys. 201 (1995) 287.

[9] F. Güthe, R. Locht, B. Leyh, H. Baumgärtel, K.M. Weitzel, J. Phys. Chem. A 103 (1999) 8404.

[10] R. Locht, J. Momigny, in: F. Lahmani (Ed.), Photophysics and Photochemistry above 6 eV, Elsevier, Amsterdam, 1985, p. 171.

[11] W. Zhang, G. Cooper, T. Ibuki, CE. Brion, Chem. Phys. 137 (1989) 391.

[12] W. Zhang, G. Cooper, T. Ibuki, CE. Brion, Chem. Phys. 151 (1991) 343.

[13] W. Zhang, G. Cooper, T. Ibuki, CE. Brion, Chem. Phys. 151 (1991) 357.

[14] W. Zhang, G. Cooper, T. Ibuki, CE. Brion, Chem. Phys. 153 (1991) 491.

[15] J.W. Au, G.R. Burton, CE. Brion, Chem. Phys. 221 (1997) 151.

[16] S. Stokes, A.B.F. Duncan, J. Am. Chem. Soc. 80 (1958) 6177.

[17] L. Edwards, J.W. Raymonda, J. Am. Chem. Soc. 91 (1969) 5937.

[18] P. Sauvageau, R. Gilbert, P.P. Berlow, C. Sandorfy, J. Chem. Phys. 59 (1973) 762.

[19] C.Y.R. Wu, L.C. Lee, D.L. Judge, J. Chem. Phys. 71 (1979) 5221.

[20] T.N. Olney, G. Cooper, W.F. Chan, G.R. Burton, CE. Brion, K.H. Tan, Chem. Phys. 189 (1994) 733.

[21] R. Locht, B. Leyh, W. Denzer, G. Hagenow, H. Baumgärtel, Chem. Phys. 155 (1991) 407.

[22] W.R. Harshbarger, M.B. Robin, E.N. Lassettre, J. Electr. Spectr. Related Phenom. 1 (1973) 319.

[23] L. Karlsson, R. Jadrny, L. Mattsson, F.T. Chau, K. Siegbahn, Phys. Scripta 16 (1977) 225.

[24] G. Bieri, L. Åsbrink, W. Von Niessen, J. Electr. Spectr. Related Phenom. 23 (1981) 281.

[25] J.W. Gauld, L. Radom, J. Phys. Chem. 98 (1994) 777.

[26] C.L. Lugez, D. Forney, M.E. Jacox, K.K. Ikura, J. Chem. Phys. 106 (1997) 489.

[27] G. Herzberg, Molecular Spectra and Molecular Structure. III. Electronic Spectra and Electronic Structure of Polyatomic Molecules, Van Nostrand, Princeton, NJ, 1967.

[28] M.J. Frisch, G.W. Trucks, H.B. Schlegel, P.M.W. Gill, B.G. Johnson, M.A. Robb, J.R. Cheeseman, T.A. Keith, G.A. Petersson, J.A. Montgomery, K. Raghavachari, M.A. Al-Laham, V.G. Zakrzewski, J.V. Ortiz, J.B. Fores-man, J. Cioslowski, B.B. Stefanov, A. Nanayakkara, M. Challocombe, C.Y. Peng, P.Y. Ayala, W. Chen, M.W. Wong, J.L. Andres, E.S. Replogle, R. Gomperts, R.L. Martin, D.J. Fox, J.S. Binkley, D.J. Defrees, J. Baker, J.P. Stewart, M. Head-Gordon, C. Gonzalez, J.A. Pople, GAUSSIAN 94 (Revision D.4) Gaussian Inc., Pittsburgh, PA, 1996.

[29] C. Møller, M.S. Plesset, Phys. Rev. 46 (1934) 618.

[30] R. Krishnan, J.A. Pople, Int. J. Quant. Chem. 14 (1978) 91.

[31] W.J. Hehre, R. Ditchfield, J.A. Pople, J. Chem. Phys. 56 (1972) 2257.

[32] T. Clark, J. Chandrasekhar, G.W. Spitznagel, P.v.R. Schleyer, J. Comp. Chem. 4 (1983) 294.

[33] A.P. Scott, L. Radom, J. Phys. Chem. 100 (1996) 16502.

[34] G. Herzberg, Molecular Spectra and Molecular Structure. II. Infrared and Raman Spectra of Polyatomic Molecules, Van Nostrand, New York, 1945.

[35] R.L. Martin, E.R. Davidson, Mol. Phys. 35 (1978) 1713.

[36] E.R. Cohen, B.N. Taylor, J. Phys. Chem. Ref. Data 37 (1973) 663.